

LONG-TERM OPTICAL VARIABILITY OF RADIO-SELECTED QUASARS FROM THE *FIRST* SURVEY

DAVID J. HELFAND

Astronomy Dept., Columbia University, New York, NY 10027, djh@astro.columbia.edu

REMINGTON P.S. STONE

Lick Observatory, Mt Hamilton, CA 95140 rem@ucolick.org

BETH WILLMAN

Department of Astronomy, University of Washington, Seattle, WA 98195-1580,
 willman@orca.astro.washington.edu

RICHARD L. WHITE

Space Telescope Science Institute, 3700 San Martin Dr., Baltimore, MD 21218, rlw@stsci.edu

ROBERT H. BECKER

Physics Dept., University of California, Davis, CA 95616
 and IGPP/Lawrence Livermore National Laboratory, bob@igpp.llnl.gov

TREVOR PRICE & MICHAEL D. GREGG

Physics Dept., University of California, Davis, CA 95616

RICHARD G. MCMAHON

Institute of Astronomy, Madingley Road, Cambridge CB3 0HA, UK

To be published in the Astronomical Journal, 2001 April 1

ABSTRACT

We have obtained single-epoch optical photometry for 201 quasars, taken from the *FIRST* Bright Quasar Survey, which span a wide range in radio loudness. Comparison with the magnitudes of these objects on the POSS-I plates provides by far the largest sample of long-term variability amplitudes for radio-selected quasars yet produced. We find the quasars to be more variable in the blue than in the red band, consistent with work on optically selected samples. The previously noted trend of decreasing variability with increasing optical luminosity applies only to radio-quiet objects. Furthermore, we do not confirm a rise in variability amplitude with redshift, nor do we see any dependence on radio flux or luminosity. The variability over a radio-optical flux ratio range spanning a factor of 60,000 from radio-quiet to extreme radio-loud objects is largely constant, although there is a suggestion of greater variability in the extreme radio-loud objects. We demonstrate the importance of Malmquist bias in variability studies, and develop a procedure to correct for the bias in order to reveal the underlying variability properties of the sample.

Subject headings: quasars:general — methods:statistical — surveys

1. INTRODUCTION

Variability on timescales ranging from hours to decades has been one of the defining characteristics of active galactic nuclei (AGN) since their discovery nearly forty years ago. These changes in the source flux received at Earth can arise from many causes: variability in the source's central engine, changes in a relativistic beam's orientation or velocity, changes in absorption along the line of sight to the active nucleus, gravitational microlensing, and interplanetary or interstellar scintillation. As such, AGN variability provides an important diagnostic in studies of the physics of the central engine, the nuclear environment, the properties of the material along the line of sight, and, ultimately, of the evolution of the AGN population.

Twenty-five years ago, Grandi and Tifft (1974) published the first compilation of quasar variability studies. Citing 92 references to previous work, they listed photographic and photoelectric photometry for a heterogeneous sample of 86 bright ($B < 18$) quasars, concluding that typical uncertainties in quasar optical magnitudes result-

ing from long-term variability were ~ 0.25 magnitudes. A conference devoted exclusively to AGN variability – on all timescales and throughout the electromagnetic spectrum – summarized the status of the subject at the beginning of the last decade (Miller and Wiita 1991). Since that time, over a dozen major studies of optical variability have appeared (Table 1), covering timespans up to thirty years and including over 1000 objects. Most, however, include only optically selected quasars; Smith et al. (1993), Netzer et al. (1996), Sirola et al. (1998), and Garcia et al. (1999) are the exceptions with a combined total of 160 radio-loud quasars in their samples. Considerable disagreement remains regarding the correlation of variability amplitude with quasar power, redshift, and other quasar properties (see the references in Table 1).

We are in the process of compiling a very large sample of bright quasars using the Very Large Array (VLA)¹ *FIRST* survey to select candidates from the POSS-I plates for optical spectroscopic followup. As part of this program, we have obtained current photometric B and R magnitudes for over 200 confirmed quasars, providing variability es-

¹The VLA is part of the National Radio Astronomy Observatory which is operated by Associated Universities, Inc., under cooperative agreement with the National Science Foundation.

TABLE 1
SUMMARY OF LONG-TERM QUASAR OPTICAL VARIABILITY STUDIES

Paper (date)	Maximum Timescale (yrs)	Sample	Colors	Number of Objects	Number of Observations	Number of Radio- Selected Objects
Netzer & Sheffar (1983)	31	84 deg ²	O	64	2	0
Cristiani et al. (1990)	7	SA 94	B	90	15	0
Giallongo et al. (1991)	4-11	Braccesi + SA57	B	55	7-9	0
Ciamati et al. (1993)	2	small area	U,F,J	52	3	0
Smith et al. (1993)	21	radio-loud	B, Ph	60	40-100	60
Hook et al. (1994)	16	SGP	B _J	300	12	0
Trevese et al. (1994)	15	SA 57	B _J	35	11	0
Hawkins (1996)	15	south	III A _J	71	~ 10	few
Cristiani et al. (1996)	5	SA 94	B	180	10	0
Netzer et al. (1996)	6	north	B	44	25-50	44
Cristiani et al. (1997)	8	SA 94	B,R	149	8	0
Trevese et al. (1997)	6	SA 57	U,B,F	26	24	0
Sirola et al. (1998)	4-7	Las Campanas	V,R	151	5-10	21
Garcia et al. (1999)	3	V < 16.5	V	50	5-10	35
Giveon et al. (1999)	7	PG	B,R	42	30-60	0
This work	48	FBQS	B,R	202	2	202

timates on proper timescales of 10–45 years for a large quasar sample spanning a broad range in radio loudness. In section 2, we briefly describe the *FIRST* quasar survey and the selection from it of our variability sample. We go on to describe the photometric observations and their reduction (§3) as well as the procedures used to calibrate the photometry of the archival POSS-I data (§4). Section 5 presents our results including a comparison with previous work and an analysis of the dependence of variability amplitudes on radio loudness, redshift and luminosity, as well as the important effect Malmquist bias has on the distribution of the magnitude variations. We conclude with a summary of our results.

2. THE *FIRST* BRIGHT QUASAR SURVEY

The *FIRST* Bright Quasar Survey (FBQS) has recently been described in detail by White *et al.* (2000). Briefly, the survey is based on a comparison of the radio catalog from the VLA *FIRST* survey (Becker *et al.* 1995; White *et al.* 1997) and the Cambridge Automated Plate Machine scans of the Palomar Observatory Sky Survey-I (POSS-I) plates (APM – McMahon and Irwin 1992; McMahon *et al.* 2000). All optical objects brighter than E (red) magnitude 17.8 (after corrections for extinction)² classified as stellar on at least one of the two POSS-I plates, which are bluer than $O - E = 2.0$ and lie within $1.2''$ of a radio source, are selected as quasar candidates. Spectroscopic followup has demonstrated that over 55% of these objects are quasars, with another $\sim 10\%$ classified as BL Lac objects; the remaining sources are a mix of narrow-line AGN, HII galaxies, and radio galaxies lacking emission lines. Over 700 quasars and BL Lacs have been found in the first ~ 2700 deg² of the survey; $\sim 75\%$ are newly discovered objects.

For our followup program of optical photometry, 201 quasars were selected at random from both the portion of the north Galactic cap survey reported in White *et al.* (2000) and its extension to the *FIRST* equatorial strip in the south Galactic cap (Becker *et al.* 2001). Suitability for the Right Ascension range of each scheduled observing run was the only selection criterion; the magnitude, radio flux density, and redshift distributions of the chosen quasars are statistically identical to these distributions for the FBQS sample as a whole. Flux densities for the sample cover a range 1.0 - 15,000 mJy, and objects with redshifts from 0.1 to 3.4 are included. The ratio of 5 GHz to 2500 Å flux densities R^* used to characterize the radio loudness of an object (Stoche *et al.* 1991) spans the range 0.3 to 22,000; objects with $R^* < 10$, generally characterized as radio-quiet quasars, constitute 46% of the sample.

3. OPTICAL PHOTOMETRY

Observations of the selected objects were carried out by one of us (RPSS) in a number of observing runs at the Lick 1-m telescope over the period 20 December 1995 through 6 June 1997. The 2048×2048 pixel Orbit CCD provides a $6'$ field of view, sufficient to include a number of stars in each image for use in calibrating the APM magnitudes.

Observations were conducted through standard B and R filters; typical integration times were 100–600 s divided into two frames to facilitate cosmic ray rejection. Standard stars from the list of Landolt (1992) were observed at least twice per night to solve for the extinction correction. Conditions during the observations ranged from photometric to light cirrus.

The data were reduced using standard IRAF routines for flat-fielding, cosmic ray removal, calibration and photometry. In particular, the IRAF task PHOT was used to perform aperture photometry on both the quasar target and all other stellar objects of similar magnitude in the field.

4. CALIBRATION OF THE APM MAGNITUDES

The preliminary photometric calibration of the APM POSS-I scans currently in use is described in some detail in McMahon *et al.* (2000). For stellar objects, the global rms photometric uncertainty is 0.5 magnitudes in the range of interest here ($15 < O, E < 19$), a precision insufficient for detecting the expected variability amplitudes for most quasars. Thus, we began by using our CCD photometry in the 201 quasar fields to calibrate each of the 53 POSS-I plates on which our objects were found.

There are from 1 to 15 quasar fields per plate. In each field, we selected isolated stellar objects with $13 < B, R < 19$ for use in forming a sample for photometric calibration. The magnitudes in the two CCD exposures for each star were compared; if they differed by more than 0.2 magnitudes, the star was discarded. The stars were then matched to the APM catalog with a matching criterion of $10''$ (in order to account for proper motion over the ~ 45 -year interval between the POSS-I and our observations); any star with no match was discarded. If two stars matched within this radius, the nearer one was chosen unless it differed in brightness by more than 2 magnitudes. These procedures yielded a database of 1695 stars.

We then performed an iterative, linear least-squares fit to the magnitude differences ($B - O, R - E$) as a function of O, E magnitude in order to derive a magnitude-dependent calibration for each pair of plates; stars lying more than 3σ from the best fit on either plate were deleted from the database in order to eliminate variable stars, mismatched stars, images affected by cosmic ray hits, etc. We required a minimum of five stars per plate for an acceptable calibration; the median was 16 stars per plate, with the best covered regions having more than 80 stars per plate. The mean (and median) rms values from the fits to both sets of plates are 0.15 magnitudes; the fit for the POSS-I O plate 1146 is displayed in Figure 1. The corrections were then applied to the O and E magnitudes for each quasar. We estimate that the combined uncertainty in the magnitude differences due to measurement and calibration errors is 0.17 magnitudes for both the red and blue.

As an additional check on the calibration procedure, we compared our CCD-corrected magnitudes with the APS-corrected magnitudes which we have derived for the entire

²The initial selection for the FBQS came from the APM magnitudes. Subsequent calibration of these magnitudes using the APS scans (see McMahon *et al.* 2000 for details) led to a small number of objects already spectroscopically confirmed as quasars being dropped from the sample presented in White *et al.* (2000) because their revised POSS-I magnitudes fell slightly below the $R = 17.8$ threshold. This program, however, was begun before the recalibration. Thus twenty-one of the sources observed have POSS-I magnitudes slightly fainter than $R = 17.8$ as can be seen in column 9 in Table 2. Eight of these have been published in Gregg *et al.* (1996), while the remainder appear here for the first time.

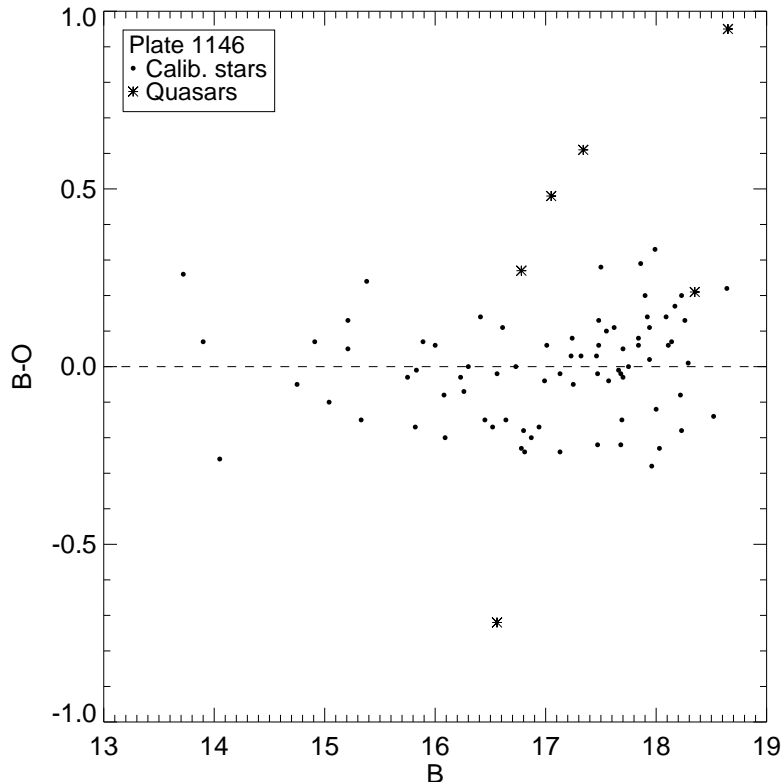


FIG. 1.— The calibration results for the POSS-I *O* plate 1146. Stars selected from our CCD images for use in the calibration are represented by dots, while quasars are shown as asterisks. The rms for the 78 stars is 0.14 mag; note the substantially higher scatter for the quasars, as well as the marked tendency for the quasars to be fainter (positive $B - O$) at the current epoch.

APM/*FIRST* identification catalog described in McMahon et al. (2000). The distribution of corrections was very similar; since the scatter in the APS magnitudes was slightly larger, we used our CCD plate-by-plate calibrations when they were available. For eight of our quasars, there were too few calibration stars per plate, and the APS magnitudes were used; these sources are flagged in Table 2.

5. LONG-TERM QUASAR VARIABILITY

5.1. Photometric results

In Table 2, we present the calibrated O , B , R , and E magnitudes for our 201 quasars. Each source's *FIRST* coordinates are given in the first two columns. The next two columns list the dates of observation for the POSS I plates (both colors were taken on the same night) and for our CCD observations, followed by the calibrated magnitudes and $B - O$, $R - E$ variations (positive $B - O$, $R - E$ values mean the source is fainter now than when it was first detected on the POSS I plates). We also include the *FIRST* peak and integrated 20cm flux densities, the measured redshift (from White et al. (2000), Becker et al. (2001), Gregg et al. (1996) and our own unpublished values for the remaining objects with $E > 17.8$), and values for the absolute blue magnitude, radio luminosity, and $\log R^*$, the radio loudness parameter; an $H_o = 50 \text{ km s}^{-1} \text{ Mpc}^{-1}$, $\Omega = 1$, $\Lambda = 0$ cosmology is assumed throughout. Note that the radio luminosities are for the radio core *only* and do not include flux from any extended lobes. The final column contains a radio morphology flag; about 10% of

the sources are classical double-lobed sources, while most of the remainder are point-like at the $\sim 5''$ resolution of the *FIRST* survey.

By far the most variable object in the sample is the EGRET source 4C38.41 (FIRST J131059.4+323334), a well-known Optically Violent Variable which was 4.45 and 4.17 magnitudes brighter in the E and O bands, respectively, in 1950 than when we observed it in 1996. Since Barbieri et al. (1977) saw this object change from $B=15.85$ to $B=19$ over the course of four years, the large variation we report is not unexpected. The only other object which varied by more than 1.5 magnitudes in either band is the low-redshift ($z = 0.28$), core-dominated, flat-spectrum quasar B1719+357 for which $B - O = 1.98$.

In all, 30 objects (15%) varied by at least a factor of 2 in at least one band. Of these, only four have been reported previously in the literature as optical variables. For the sample as a whole, there is a large bias toward objects having faded since their POSS-I detections; a detailed analysis of this effect, a manifestation of Malmquist bias, is given below, following which we present the results of comparing long-term variability with other quasar properties.

5.2. Skewness of the δm distribution

Figure 2 shows the distributions of the change in quasar magnitude ($\delta m = m_{\text{CCD}} - m_{\text{POSS}}$) in the red and blue bands. The distributions are clearly skewed, with many more quasars found to be dimmer in the CCD data than

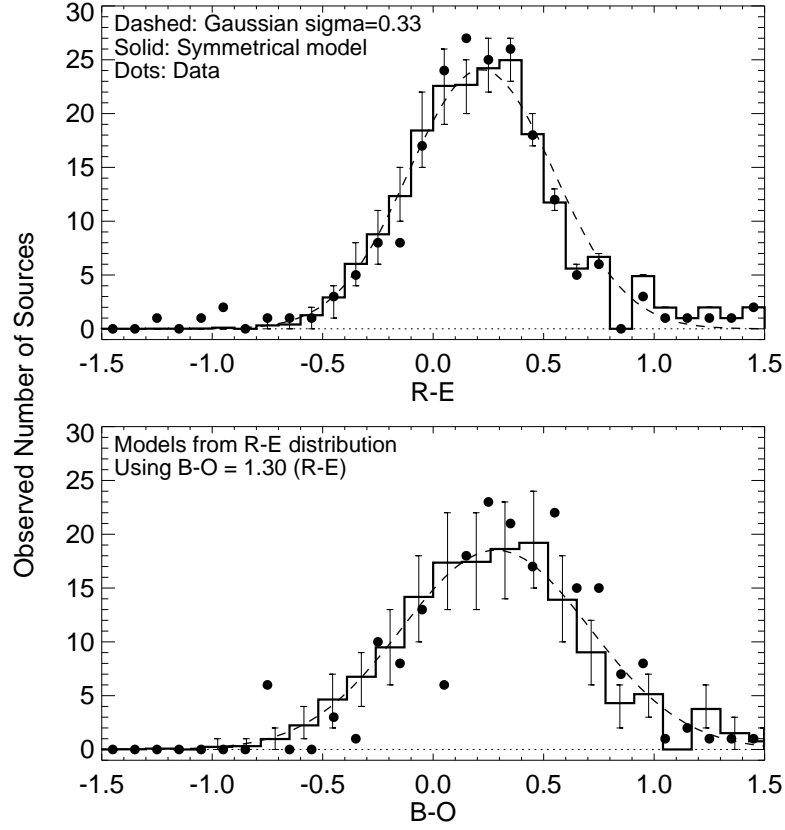


FIG. 2.— Observed distribution of magnitude change $\delta m = m_{\text{CCD}} - m_{\text{POSS}}$ for quasars in our sample. Objects on the right were fainter in the current CCD observations. The histogram is skewed due to Malmquist bias (see text for discussion.) The dots are the observed counts, and the solid line shows the predicted counts in bins (with 1σ uncertainty error bars) from a symmetrical, Malmquist-corrected model. The dashed line is a Gaussian distribution having the same rms as the model distribution. (a) Red magnitude differences ($m_R - m_E$). The Gaussian width is $\sigma = 0.33$. Error bars account for the use of these same data to compute the model values and show the expected range for data points about that mean. (b) Blue magnitude differences ($m_B - m_O$). The model (both histogram and Gaussian) are derived from the red delta-magnitude distribution using the relation $B - O = 1.3(R - E)$. In this case the model is derived completely independently from the data, so the error bars show the expected range for these data about the mean due to Poisson statistics.

are found to be brighter. This asymmetry is the result of Malmquist bias (Malmquist 1924) in the FBQS sample. Because the quasar number counts increase steeply with magnitude, a disproportionate fraction of quasars near the FBQS magnitude limit are included in the sample because small brightness fluctuations at the time of the POSS-I observation moved them above the optical threshold for inclusion in the sample.

It is relatively straightforward to correct the observed δm distribution, $P_{obs}(\delta m)$, for Malmquist bias and thus determine the true distribution, $P_{true}(\delta m)$. Let m be the true (current-epoch CCD) magnitude of the quasar, m_0 be the magnitude brightness limit of the FBQS sample, and $N(m)$ be the cumulative number of quasars brighter than m . For $\delta m > 0$, the quasars were brighter on the POSS-I plates than they are currently, so the FBQS sample was effectively looking deeper in the $N(m)$ distribution and thus included more objects. The observed magnitude distribution is

$$P_{obs}(\delta m) = \frac{P_{true}(\delta m)N(m_0 + \delta m)}{\int_{-\infty}^{\infty} P_{true}(\delta m)N(m_0 + \delta m)d\delta m} \quad (1)$$

The factor in the denominator simply normalizes P_{obs} so that its integral is unity.

For quasars at $V \sim 17.5$, the cumulative number distribution is approximately exponential:

$$N(m) = N_0 e^{(m-m_0) \ln F} \quad (2)$$

where F is the factor by which the counts increase for a 1 magnitude change ($F \simeq 7.6$, La Franca and Cristiani 1997). Thus the observed distribution is

$$P_{obs}(\delta m) = \frac{P_{true}(\delta m)e^{\delta m \ln F}}{\int_{-\infty}^{\infty} P_{true}(\delta m)e^{\delta m \ln F}d\delta m} \quad (3)$$

This integral can be evaluated analytically for a Gaussian distribution. If $P_{true} = \exp(-\delta m^2/2\sigma^2)$ then

$$P_{obs}(\delta m) = \exp(-[\delta m - \sigma^2 \ln F]^2/2\sigma^2) \quad (4)$$

A Gaussian distribution simply has its mean shifted by $\sigma^2 \ln F = 2.03\sigma^2$ for $F = 7.6$.

More generally, it is safe to assume that the true distribution of δm is symmetrical about zero. Using this (weak) assumption, we can symmetrize the observed histogram of δm . Consider two histogram bins symmetrically placed about zero: $|\delta m - \delta m_h| < b$ and $|\delta m + \delta m_h| < b$, where the bins are centered at $\pm \delta m_h$ and the bin width is $2b$. Let the number of objects in each δm bin be N_+ and N_- . By the symmetry assumption, the true distribution has the same expected number of objects in each bin, \bar{N} . If the bin width is small, the expected number of objects $E(N)$ in the observed distribution is modified by a Malmquist bias factor W :

$$E(N_+) = \bar{N}W_+ = \bar{N} \exp(\delta m_h \ln F) \quad , \text{ and} \quad (5)$$

$$E(N_-) = \bar{N}W_- = \bar{N} \exp(-\delta m_h \ln F) \quad . \quad (6)$$

The most accurate estimator of the true number of objects in the bin is then

$$\bar{N} = \frac{N_+ + N_-}{W_+ + W_-} \quad (7)$$

Some straightforward algebra will convince the reader that this gives the correct answer in the case of a Gaussian distribution (except for a constant normalization factor, which can be computed directly from \bar{N} .) The uncertainty in the estimator \bar{N} is easily determined, since it has a Poisson noise distribution scaled by the $W_+ + W_-$ factor.

A subtle point is that the observed blue magnitude differences are biased only through their coupling to the red magnitudes, because the red magnitude was used to define the sample. There is a weak bias that directly affects the blue due to a limit $O - E < 2$ on the colors of FBQS quasars. Thus, quasars that are near the FBQS limit $E = 17.8$ must be brighter than $O = 19.8$ to be included in the sample. However, most quasars are much bluer than this limit and so the bias in the blue δm_B distribution (which is apparent in Fig. 2) appears only because the blue variation is highly correlated with the red variation.

To understand how the bias affects the blue δm_B distribution, consider a hypothetical population of objects that do not vary at all in the red but do vary in the blue. For simplicity we also assume measurement errors are zero. At the FBQS discovery epoch, we simply select all the objects brighter than the sample magnitude limit. Some of those objects are brighter than average in the blue and some are fainter, but all are included in the sample because there is no discrimination against faint blue magnitudes. At the current epoch we would find that the blue magnitudes differ but the red magnitudes are unchanged. The observed blue δm_B distribution would consequently be symmetrical about zero, with no Malmquist bias at all.

Now consider another extreme hypothetical population, where both the red and blue magnitudes of the objects vary but the blue magnitude is completely determined by the red magnitude, such that $\delta m_B = \alpha \delta m_R$ where α is a constant. In this case, the selected sample is biased by brightness fluctuations that bring objects with brighter R magnitudes into the sample; those objects also have brighter B magnitudes. At the current epoch, we therefore find that many objects have dimmed in both B and R according to the hypothesized linear relationship. In this case the observed δm_R distribution is related to the true distribution as derived in equations (1)–(7) above, and the δm_B distribution is merely a rescaled version of the δm_R distribution. For example, if $\alpha = 2$, then the δm_B distribution will be twice as wide, shifted twice as far from zero, and (to conserve counts) half as high as the δm_R distribution. This result is *not* the same as if the blue magnitudes were themselves Malmquist-biased; in that case, when the distribution is twice as wide, it is shifted four times as far from zero (Eq. 4) rather than twice as far.

The real case is, of course, between these two extremes, with the blue variation having components that are both correlated with and independent of the red variation. Fig. 3 shows that δm_B is in fact strongly correlated with δm_R . The best-fit line through the points, allowing for measurement errors in both coordinates, is $\delta m_B = 1.30 \delta m_R$. If we assume that the uncertainty in δm_R is 0.17 (an estimate of the combined measurement errors in E and R), then the scatter about the best fit line

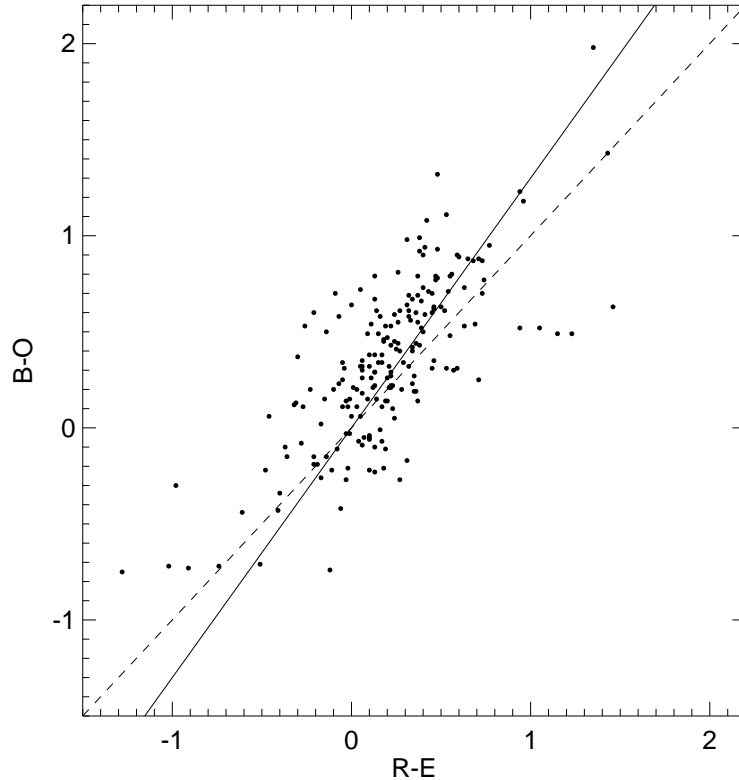


FIG. 3.— A comparison of the $R-E$ and $B-O$ variations for our quasar sample. The dashed line indicates identical variations in the two colors, while the solid line has the best fit slope of 1.30. The most highly variable source ($\delta m_R \sim 4.5, \delta m_B \sim 4.2$) falls outside the plot. The magnitudes are strongly correlated, with higher variability amplitudes in the blue.

indicates that the uncertainty in $\delta m_B \simeq 0.24$ in order that the χ -square of the fit be approximately 1 per degree of freedom. Since the measurement errors on B and O are similar to those in the red, the implied “intrinsic” scatter in $\delta m_B \simeq 0.17$. In other words, the portion of the blue variability that is uncorrelated with the red variability is relatively modest and is of the same order as the measurement error.

Figure 4 shows the δm distributions for both the red and blue symmetrized and corrected for the Malmquist bias (see Eq. 7). The predictions from the symmetrical model are in good agreement with the data. Note in particular the reasonably good agreement with the blue distribution; since the model in this case was derived from the red δm_R data, there are no free parameters in the fit. The red distribution was converted to a blue model simply by scaling the δm values by a factor 1.30, as indicated by the fit in Fig. 3. A Gaussian with the same rms as the model distribution is also shown and appears to be quite a good representation for the bulk of the distribution, although there is certainly a non-Gaussian tail of high-amplitude variables.

The predictions of the symmetrical model (and the associated Gaussian) are also shown in Fig. 2 where they are overlain on the observed (biased) counts. This predicted distribution is obtained by multiplying the true symmetrical distribution by the Malmquist factor W from Eq. (4). As was mentioned above, the biased Gaussian distribution is just a shifted Gaussian with the same width. Note

that the Gaussian in Fig. 2a has only *one* free parameter (the width) because the shift is *specified* by the width and the normalization is determined by the total number of quasars; thus the good agreement with the observational distribution supports both the general approach adopted here and the idea that there is a roughly Gaussian underlying distribution of amplitude fluctuations.

In the following section we examine the dependence of variability on various quasar properties (e.g., redshift and radio-loudness). Malmquist bias affects all of these measurements. The correction procedure derived above can also be applied to any subset of the data to determine a Malmquist-corrected rms value for the variability of that subset. The approach we have adopted is to compute the symmetrized distribution for the subset (typically objects having some property falling within a moderately narrow range) and then calculate the rms from that distribution. From the analysis of the whole sample above, this approach is seen to give a good measurement of the width of the (approximately Gaussian) histogram. We exclude the single object that varied by 4 magnitudes (4C38.41) from these calculations since it produces a wild outlying value for the rms of any bin into which it falls.

5.3. Correlation with other quasar properties

Figure 3 compares the variability amplitudes for the red and blue bands. The correlation between the two bands is apparent, as is the fact that the average variability amplitude is higher in the blue. This trend has been seen in pre-

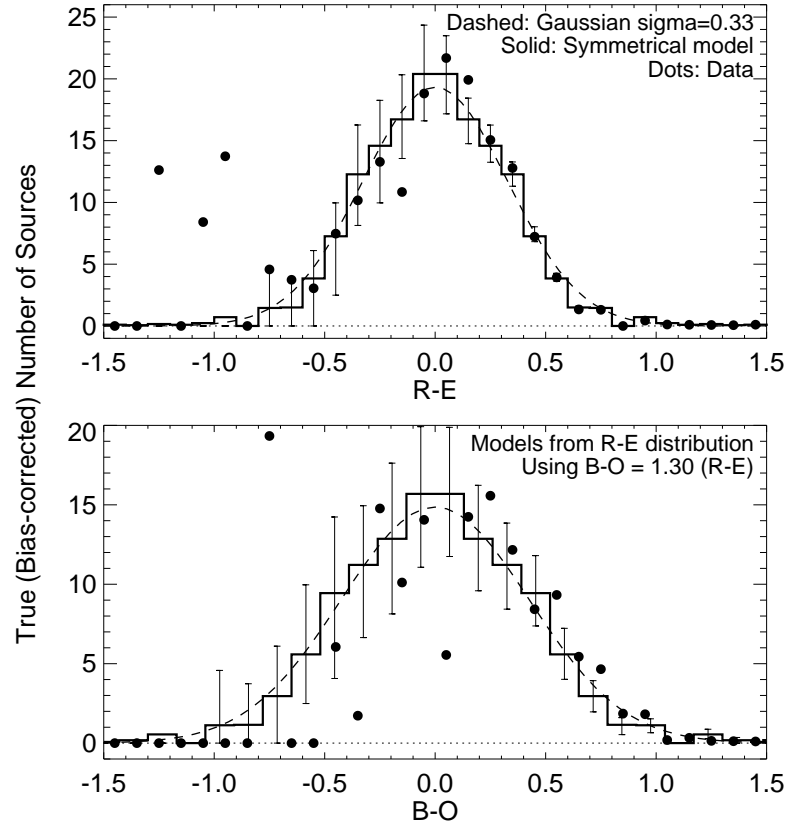


FIG. 4.— The distribution of magnitude differences corrected for Malmquist bias under the assumption that the true distribution is symmetrical about zero. As in Fig. 2, the dots are the observed counts corrected for the Malmquist factor in each bin, the solid line is the true distribution of δm , and the dashed line is a model Gaussian; in both panels, the models are derived from the red data. (a) Red magnitude differences. (b) Blue magnitude differences.

vious optically-selected samples; e.g., Figure 2 in Trevese et al. (1997) suggests that for a factor of two change in wavelength, $\delta m_B - \delta m_R \sim 0.11$. For our sample, the mean difference between the variability amplitudes is 0.13 mag. When the Malmquist bias is removed, the rms variations in the blue and red are 0.45 mag and 0.33 mag, respectively (Fig. 2). If we subtract in quadrature the 0.17 mag rms contributed by calibration errors (§4), the quasar blue and red rms values are 0.42 and 0.28 magnitudes. Thus the bias-corrected rms difference is 0.14 mag, in good agreement with Trevese et al.

In Figure 5, we show the distribution of δm as a function of redshift. We have made no correction for emission lines in our analysis; in that B, O and R, E are not identical bands, strong lines entering the bands at slightly different redshifts could be a cause for concern. We have marked the locations at which MgII, CIV, and Ly α enter and leave the POSS-I bands; no significant anomalies are seen. While it is possible that a few objects with very strong lines could have their δm values affected by line emission, it does not appear that the statistical conclusions derived from our sample will be biased by this effect. Note again the strong preference for positive δm values induced by the Malmquist bias. However, the amplitude of the variability in both bands is independent of z . Binning the objects in redshift intervals of 0.5, we find, for example, that $\langle \delta m_R \rangle$ differs by only 0.01 mag in the $z < 0.5$ and $z > 3$ bins, and in none of the seven bins is the mean value more than 1.5σ from the overall mean value of 0.33 when correction for the Malmquist bias is applied (see above). These results are inconsistent with the majority of recent studies on optically selected samples (e.g., Fernandes, Aretxaga, and Terlevich 1996 and references therein). Given the complex interaction of k-corrections, wavelength-dependent variability, the redshift-luminosity correlation in a flux-limited sample, etc., it is difficult to assess the significance of this disagreement.

The range of redshifts in the sample (and the range of time over which the data at the two epochs were collected) means the proper time intervals sampled range from 10 to 45 years. The mean values of the variability amplitudes for proper times less than, and greater than, 20 years are identical to within 0.02 and 0.01 magnitudes, the respective errors in the means for the blue and red bands.

Figures 6a and b illustrate the size of the effect Malmquist bias can introduce when searching for correlations between variability amplitude and other quasar properties. We show the median amplitudes over a span of 10^7 in radio luminosity both before and after correcting for the Malmquist bias using the prescription outlined above. While before correction, the plots are noisy but suggest a positive correlation with luminosity in the R band, the corrected values are flat, with all points consistent with the median value to within less than 2σ . We also find that variability amplitude is uncorrelated with optical apparent magnitude when Malmquist-corrected distributions are employed.

The high resolution of the *FIRST* survey allows us to comment on the radio morphology dependence of the variability. The FBQS selection criteria require a radio component coincident with the optical counterpart, so our sur-

vey may be partially incomplete for sources with very weak core components and dominant radio lobes (classical FR-II radio doubles), although our recent extension of the FBQS to include candidate doubles suggests the incompleteness is less than 5% (Becker et al. 2001). Furthermore, it is possible that the lobe components for some of our identified quasars have been resolved out in our high-resolution radio observations, although, again, the fraction of such objects is small, since most have not been found to have extended components in the much lower-resolution NVSS survey (Condon et al. 1998).

In total, roughly 10% of the sources in the current sample show extended emission, and most of these are FR-II objects. We have computed the $\text{rms}(B - O)$ and $\text{rms}(R - E)$ values for the single and complex sources separately and, surprisingly, find that those sources with extended components are slightly *more* variable; e.g., $\text{rms}(R - E) = 0.320 \pm 0.010$ for the single sources, while $\text{rms}(R - E) = 0.376 \pm 0.028$ for the complex objects. This result is not highly significant ($\sim 2\sigma$) but is in the opposite sense expected from standard unified models of AGN in which the sources with extended lobes are oriented roughly normal to the line of sight, while sources with bright core components have their jets beamed toward us and should thus, on average, be more variable. Given possible incompleteness in the sample and the low significance of the distinction, it is clear that a larger sample of FR-II sources would be required to draw quantitative conclusions.

Fig. 7 shows the dependence of variability amplitude on the radio-loudness parameter over a range in R^* of 10,000. The curves in the two bands are remarkably similar, and suggest a nearly constant amplitude over most of the range, with a possible turn up for the extreme radio-loud objects.

The final figure (Fig. 8) shows a three-dimensional distribution of variability amplitude as a function of both R^* and absolute magnitude. Fluctuations from the mean value of less than 1σ have been suppressed (by shrinking all values toward the mean) to emphasize the more significant features of the distribution. The trend noted by Hook et al. (1994) in their optically selected sample for variability amplitude to decrease with increasing absolute magnitude is apparent here for the objects with $R^* < 10$ (the radio-quiet portion of our sample)³, but disappears for objects with higher radio-to-optical flux ratios. The dependence of this trend on radio loudness could arise if the overall variability is composed of two parts: one due to long-term changes in the structure of the accretion disk giving rise to changes in the thermal tail of the ‘big blue bump’, and the other arising from fluctuations in the non-thermal, beamed emission. The most luminous objects with large, slowly varying disks would have a smaller amplitude of variability unless the nonthermal emission comes to dominate the optical flux; the higher amplitude variability for the radio-loudest objects, apparent in the figure, is consistent with assigning the greater variability amplitude to the beamed emission.

The decrease in variability seen here for the lowest luminosity objects is significant at the 4.9σ level (comparing $M_B > -24$ to $-24 > M_B > -28$) and has not been re-

³Comparing the radio quiet sources with $M_B < -28$ to those in the range $-28 < M_B < -24$, the rms variability amplitudes are different at the 6.1σ level.

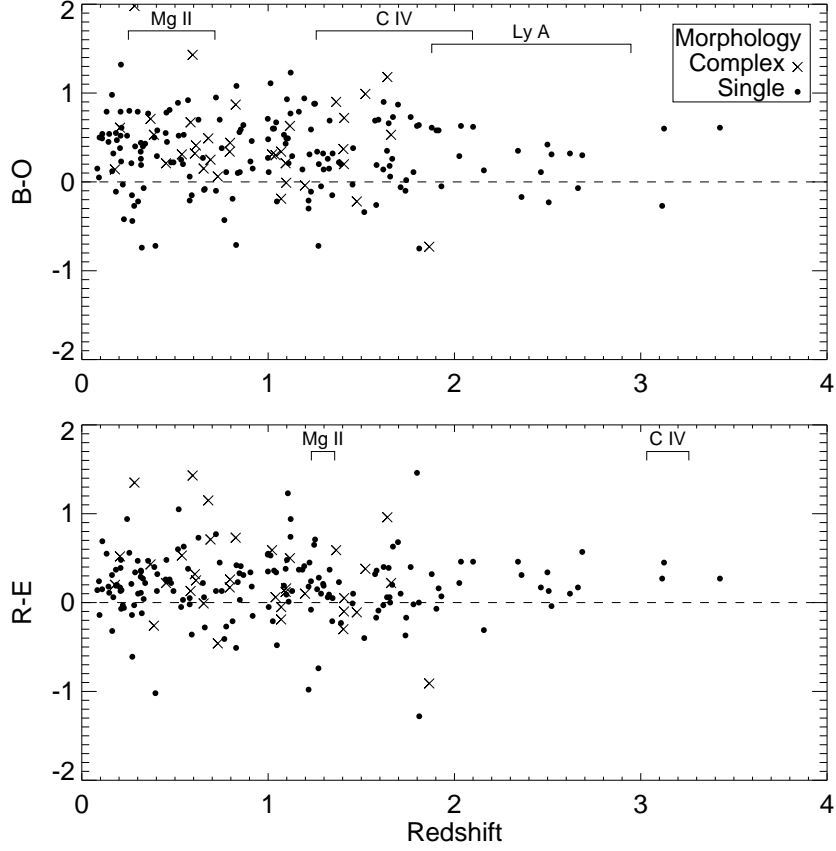


FIG. 5.— A plot of δm_R and δm_B as a function of redshift. Complex (FR II and core-jet) extended radio sources are indicated by \times symbols; simple single sources are indicated by dots. The redshifts where various strong lines enter and leave the POSS-I bands are indicated at the top of each panel. While a strong bias towards sources becoming fainter is apparent in both bands, there is no obvious trend in variability amplitude with redshift, contrary to the results from some recent optically selected samples.

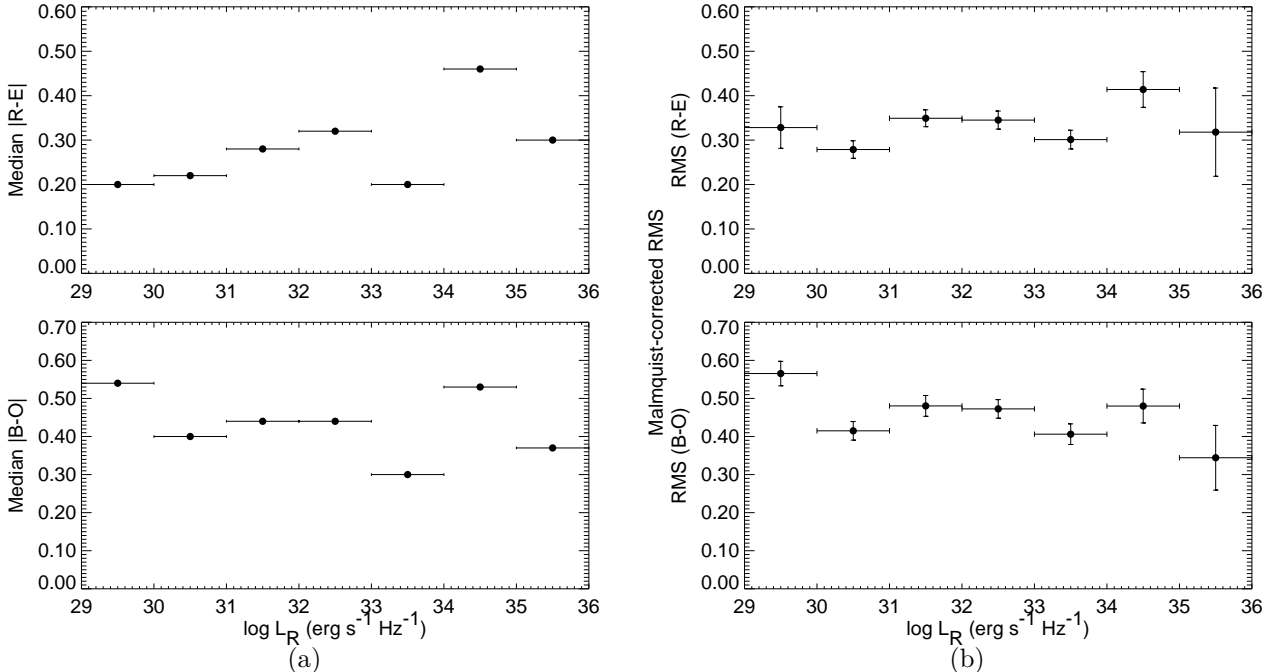


FIG. 6.— The distribution of median δm_R and δm_B as a function of radio luminosity. Fig. 6a shows this distribution before correction for Malmquist bias, while 6b shows the result of applying the correction stipulated in §5.2. After the correction, no dependence on L_r is apparent.

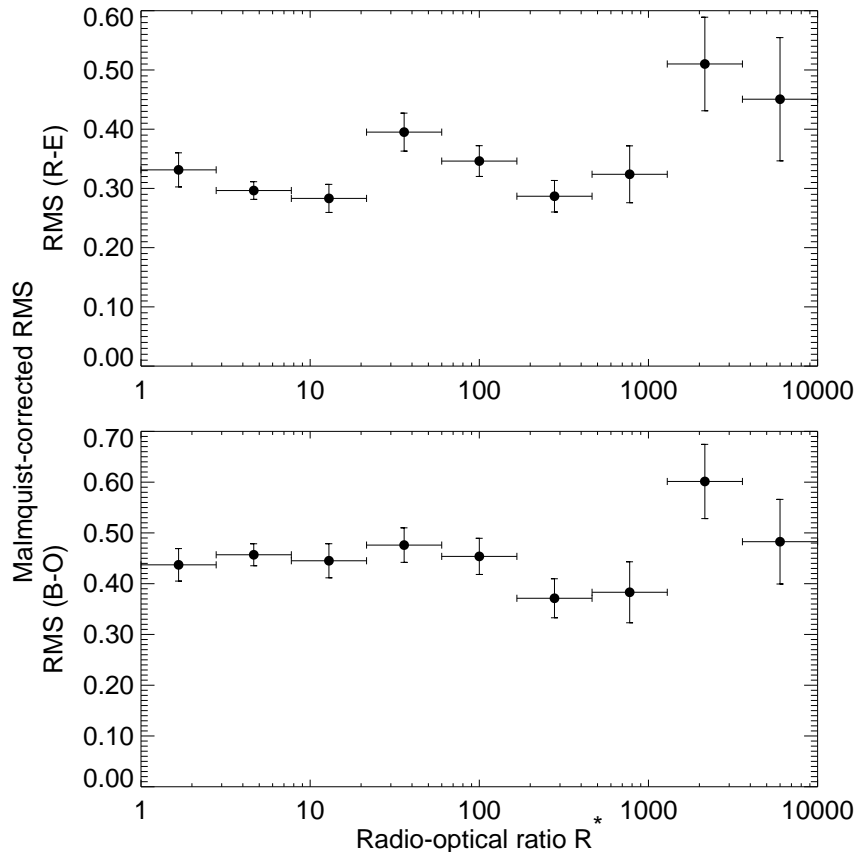


FIG. 7.— Variability amplitude is displayed as a function of the radio loudness parameter R^* (using the Malmquist-corrected rms values of δm). In both bands, the distributions are flat, with the hint of an upturn for the radio-loudest objects.

ported previously as a consequence of the exclusion from most quasar samples of objects with $M_B > -23.5$. Furthermore, the trend apparently does not continue toward lower luminosity Seyfert galaxies; in the compilation by Winkler et al. (1992), six of the seven highest amplitude variables over a four-year period are drawn from the upper half of the luminosity distribution (median luminosity $M_B = -21.2$).

6. SUMMARY AND CONCLUSIONS

We have presented a study characterizing the long-term (~ 45 yr) variability properties for a radio-selected sample of 201 quasars spanning large ranges in redshift, luminosity, and radio loudness. We find little or no dependence of the variability amplitude on radio or optical flux, radio luminosity, or redshift. We do see higher mean amplitudes in the blue band than the red band, consistent with the reported wavelength dependence in optical samples. The dependence on radio loudness is largely flat, with a slight upturn for the extremely radio-loud objects. The decrease in variability amplitude for optically luminous quasars is confined to radio-quiet objects. We also demonstrate the importance of considering Malmquist bias when characterizing the variability properties of a quasar sample, and describe a technique for correcting observed distributions of variability amplitude.

The complex interdependence of the observed variability on frequency, redshift, bolometric luminosity, radio loud-

ness, and possibly other parameters makes it difficult to draw definitive conclusions regarding the physics of the central engine or quasar evolution from a study such as this. A larger study of a carefully selected sample of FBQS objects, supplemented by a sample of much fainter *FIRST* counterparts, could provide the breadth of coverage in luminosity over a broad range of redshifts necessary to begin to untangle these effects.

The success of the *FIRST* survey is in large measure due to the generous support of a number of organizations. In particular, we acknowledge support from the NRAO, the NSF (grants AST-98-02791 and AST-98-02732), the Institute of Geophysics and Planetary Physics (operated under the auspices of the U.S. Department of Energy by Lawrence Livermore National Laboratory under contract No. W-7405-Eng-48), the Space Telescope Science Institute, the National Geographic Society (grant NGS No. 5393-094), and Columbia University. DJH is grateful for the support of the Raymond and Beverly Sackler Fund, and joins RHB and RLW in thanking the Institute of Astronomy at the University of Cambridge for hospitality during much of this work. We would also like to thank the Editor Paul Hodge and the referee Paul Wiita for stunning speed and efficiency in taking this paper from submission through refereeing, revision, and resubmission in four days. This paper is Contribution Number 689 of the Columbia Astrophysics Laboratory.

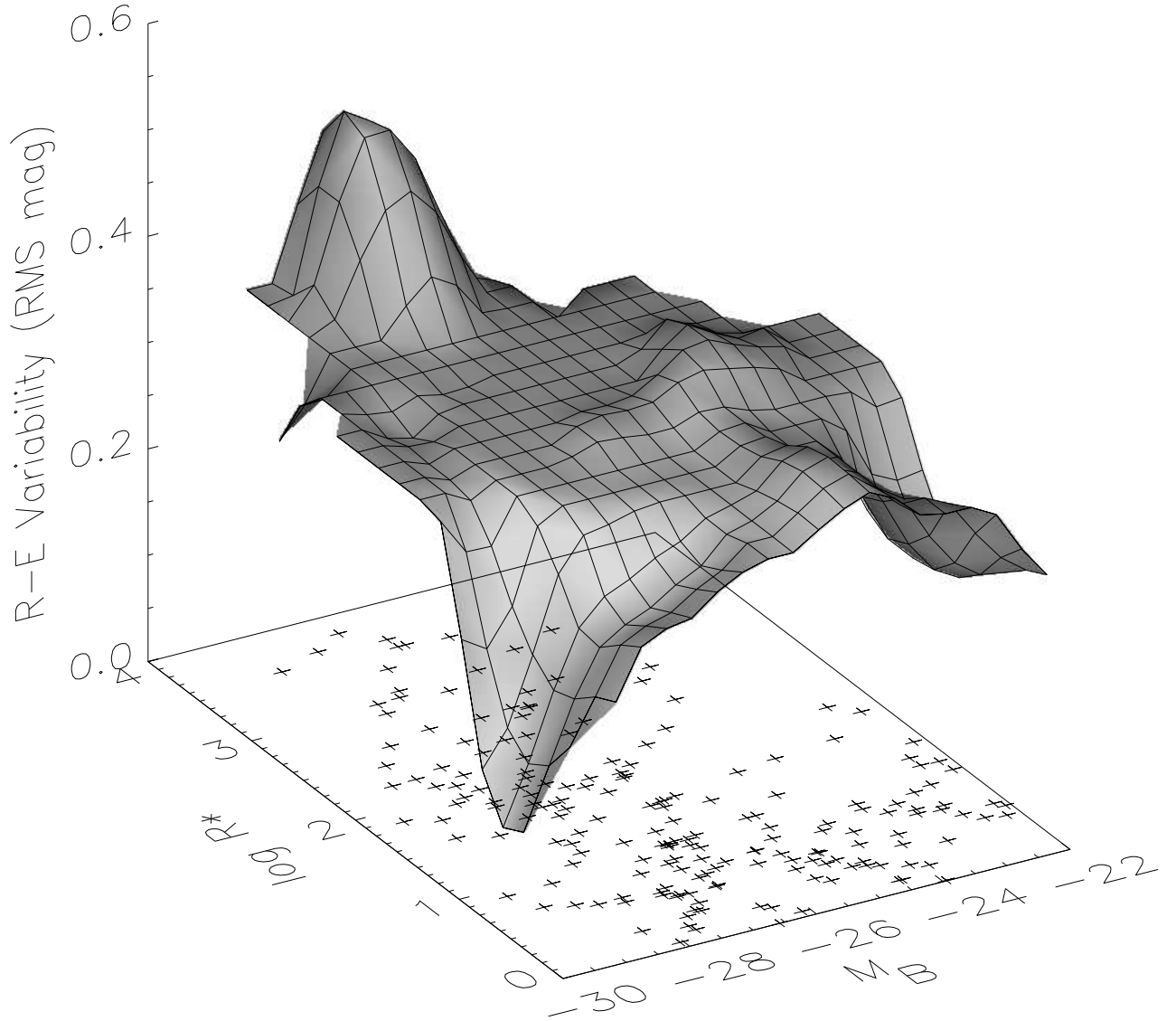


FIG. 8.— Red variability amplitude is displayed as a function of the radio loudness parameter R^* and the absolute blue magnitude. The distribution of the points on the $\log R^*$ - M_B plane is indicated. The surface has been plotted such that all variations from the mean with a significance of less than 1σ are suppressed (by shrinking the values toward the mean value, 0.34) to emphasize the more significant features of the distribution.

REFERENCES

- Barbieri, C. Romano, G., diSerego, S., and Zambon, M. 1977 *A&A* 59, 419
- Becker, R.H., White, R.L. and Helfand, D.J. 1995, *ApJ* 450, 559
- Becker, R.H. et al. 2001, *ApJ* (submitted)
- Borgeest, U. and Schramm, K.-J. 1994, *A& Ap* 284, 764
- Ciamati, A., Zamorani, G., and Marano, B. 1993, *MNRAS* 263, 236
- Condon, J.J., Cotton, W.D., Greisen, E.W., Yin, Q.F., Perley, R.A., Taylor, G.B., and Broderick, J.J. 1998, *AJ* 115, 1693
- Cristiani, S., Vio, R., and Andreani, P. 1990 *AJ* 100, 56
- Cristiani, S., Trentini, S., LaFranca, F., Aretxaga, I., Andreani, P., Vio, R., and Gemmo, A. 1996, *A& Ap* 306, 395
- Cristiani, S., Trentini, S., LaFranca, F., and Andreani, P. 1997, *A&A* 321, 123.
- Fernandes, R.C., Aretxaga, I. and Terlevich, R. 1996, *MNRAS* 282, 1191
- Garcia, A., Sodre, L., Jablonski, F.J., and Terlevich, R.J. 1999, *MNRAS* 309, 803
- Giallongo, E., Trevese, D., and Vagnetti, F. 1991, *ApJ* 377, 345
- Giveon, U., Maoz, D., Kaspi, S., Netzer, H., and Smith, P.S. 1999, *MNRAS* 306, 637
- Grandi, S.A. and Tifft, W.G. 1974, *PASP* 86, 873
- Gregg, M.D., Becker, R.H., White, R.L., Helfand, D.J., McMahon, R.G., and Hook, I.M. 1996, *AJ* 112, 407
- Hawkins, M.R.S. 1996, *MNRAS* 278, 787
- Hook, I.M., McMahon, R.G., Boyle, B.J., and Irwin, M.J. 1994, *MNRAS* 268, 305
- La Franca, F. and Cristiani, S. 1997, *AJ* 113, 1517
- Landolt, A.U. 1992, *PASP* 104, 336
- Malmquist, K.G. 1924, *Medd. Lund Astron. Obs.*, 2(32), 64
- McMahon, R.H. and Irwin, M. 1992, in *Digitised Optical Sky Surveys*, eds. H. T. MacGillivray and E. B. Thomson (Dordrecht: Kluwer), p. 417
- McMahon, R.G., White, R.L., Helfand, D.J., and Becker, R.H., 2000, *ApJ* (in press)
- Miller, H.R. and Wiita, P.J. 1991 “Variability of Active Galactic Nuclei” (Cambridge: Cambridge University Press)
- Netzer, H. and Sheffar, Y. 1983, *MNRAS* 203, 935
- Netzer, H., Heller, A., Loinger, F., Alexander, T. Baldwin, J.A., Wills, B.J., Han, M., Freuh, M., Higdun, J.L. 1996, *MNRAS* 279, 429
- Sirola, C.J. et al. 1998, *ApJ* 495, 659
- Smith, A.G., Nair, A.D., Leacock, R.J., Clements, S.D. 1993, *AJ* 105, 437
- Stocke, J.T. et al. 1991, *ApJS*, 76, 813
- Trevese, D., Kron, R.G., Majewski, S.R., Bershady, M.A., and Koo, D.C. 1994, *ApJ* 433, 494
- Trevese, D., Bunone, A., Nanni, D., Bershady, M.A., and Kron, R.G. 1997, *Mem. S.A.It.* 68, No.1, 251
- White, R.L., Becker, R.H., Helfand, D.J., and Gregg, M.D. 1997, *ApJ* 475, 479
- White, R.L. et al. 2000 *ApJ Suppl.* 126, 133
- Winkler, H., Glass, I.S., van Wyk, F., Marang, F., Jones, J.H.S., Buckley, D.A.H., and Sekiguchi, K. 1992, *MNRAS* 257, 659

TABLE 2
FIRST VARIABLE QUASAR CATALOG

RA (1)	Dec (2)	POSS1 obs (3)	CCD obs (4)	B (5)	O (6)	B-O (7)	R (8)	E (9)	R-E (10)	S_p (11)	S_i (12)	z (13)	M(B) (14)	L(R) (15)	log R^* (16)	Morphology (17)
07 17 34.48	+29 16 13.7	1953.197	1996.277	18.71	17.78	0.93	17.86	17.38	0.48	2.18	2.25	1.101	-26.7	31.8	0.65	
07 25 26.45	+29 13 40.7	1953.197	1996.277	18.45	18.13	0.32	17.44	17.39	0.05	1.64	0.97	1.346	-26.8	31.8	0.63	
07 25 50.59	+28 19 06.1	1953.197	1997.268	18.18	18.25	-0.07	17.37	17.20	0.17	37.99	38.85	2.663	-28.4	33.8	1.95	
07 29 52.34	+30 46 44.1	1953.197	1996.277	18.26	17.72	0.54	17.22	17.11	0.11	1.48	1.17	0.147	-22.1	29.9	0.57	
07 44 12.08	+29 59 06.9	1953.197	1996.277	18.93	18.06	0.87	18.59	17.91	0.68	93.72	94.90	1.697	-27.5	33.8	2.33	
07 46 04.95	+29 22 50.4	1955.279	1996.277	18.32	17.79	0.53	17.92	17.29	0.63	1.62	1.31	0.547	-25.0	31.0	0.57	
07 48 04.65	+37 40 45.7	1955.192	1996.279	19.16	18.55	0.61	18.37	18.05	0.32	2.50	2.16	1.878	-27.2	32.3	0.93	
07 49 48.24	+34 54 44.2	1955.192	1996.277	17.10	16.31	0.79	16.46	15.91	0.55	1.31	0.82	0.133	-23.3	29.7	-0.04	
07 50 47.34	+41 30 33.0	1953.279	1996.279	17.59	17.45	0.14	17.03	16.66	0.37	2.06	2.22	1.184	-27.2	31.8	0.50	
07 51 12.34	+29 19 38.2	1955.279	1996.277	16.14	15.68	0.46	15.63	15.45	0.18	1.00	1.16	0.912	-28.3	31.3	-0.46	
07 54 48.89	+30 33 54.9	1955.279	1996.277	18.07	17.63	0.44	17.44	17.18	0.26	44.75	46.47	0.796	-26.1	32.8	1.94	core-jet 12s
07 54 58.35	+29 41 54.1	1955.279	1996.277	18.67	18.05	0.62	18.29	17.83	0.46	398.19	410.00	2.100	-28.0	34.6	2.93	
07 58 00.12	+39 20 29.8	1955.159	1996.279	14.83	14.33	0.50	14.09	14.23	-0.14	10.80	11.56	0.095	-24.5	30.4	0.12	
07 59 28.30	+30 10 28.1	1955.279	1996.279	18.09	17.82	0.27	17.60	17.25	0.35	161.38	182.20	0.999	-26.4	33.6	2.58	
08 02 20.51	+30 35 42.8	1955.279	1996.279	19.42	18.24	1.18	18.85	17.89	0.96	27.81	28.55	1.640	-27.2	33.2	1.88	FRII 55s
08 04 09.30	+38 53 49.1	1955.159	1996.279	18.20	17.97	0.23	16.92	16.99	-0.07	2.88	2.68	0.211	-22.6	30.5	0.95	
08 08 49.25	+40 09 18.7	1955.159	1996.279	18.71	18.12	0.59	18.01	17.60	0.41	1.95	1.49	0.853	-25.7	31.5	0.75	
08 09 06.24	+29 12 35.3	1955.279	1996.279	17.43	17.65	-0.22	17.01	17.12	-0.11	21.48	21.87	1.476	-27.5	33.0	1.55	FRII 140s
08 09 06.52	+41 39 32.5	1955.159	1996.279	17.70	17.39	0.31	17.12	16.67	0.45	2.21	2.45	1.222	-27.3	31.9	0.51	
08 11 30.81	+39 04 11.2	1955.159	1996.279	18.71	18.05	0.66	17.92	17.53	0.39	1.62	1.82	1.647	-27.4	32.0	0.61	
08 11 48.30	+37 56 45.6	1954.227	1996.279	18.14	17.76	0.38	17.24	17.14	0.10	1.76	1.60	1.456	-27.4	31.9	0.50	
08 14 15.07	+41 23 23.4	1955.159	1996.279	18.55	18.23	0.32	17.83	17.62	0.21	5.15	4.65	1.295	-26.6	32.3	1.17	
08 21 07.63	+31 07 51.1	1955.301	1996.279	17.44	17.12	0.32	16.76	16.66	0.10	85.41	89.98	2.620	-29.5	34.1	1.87	
08 23 58.21	+36 49 53.8	1953.107	1996.279	19.31	18.41	0.90	18.54	17.95	0.59	13.64	13.64	1.365	-26.6	32.7	1.66	core-jet 20s
08 24 06.26	+33 42 45.3	1953.107	1997.184	18.46	18.20	0.26	17.85	17.74	0.11	1.93	1.08	0.317	-23.3	30.6	0.85	
08 24 55.54	+39 16 42.4	1955.159	1996.282	17.71	18.01	-0.30	16.87	17.85	-0.98	1403.96	1456.09	1.217	-26.7	34.7	3.54	
08 32 25.35	+37 07 36.1	1953.107	1996.282	16.66	16.61	0.05	16.02	15.78	0.24	11.78	11.73	0.092	-22.1	30.4	1.04	
08 32 46.94	+28 53 11.8	1955.301	1996.281	17.54	17.96	-0.42	17.02	17.08	-0.06	1.64	1.73	0.226	-22.8	30.3	0.72	
08 36 36.90	+41 25 54.6	1953.285	1996.282	18.11	17.97	0.14	17.60	17.41	0.19	424.23	443.13	1.298	-26.9	34.2	3.00	
08 40 44.40	+36 33 27.6	1953.107	1996.282	17.41	17.52	-0.11	16.42	16.50	-0.08	1.63	1.00	1.230	-27.2	31.7	0.39	
08 41 18.08	+35 44 38.4	1953.107	1996.282	17.02	16.91	0.11	16.46	16.48	-0.02	6.01	5.66	1.780	-28.7	32.6	0.66	
08 44 37.90	+41 24 31.5	1953.285	1996.282	17.74	17.22	0.52	17.50	16.45	1.05	1.58	1.38	0.520	-25.5	31.0	0.34	
08 47 16.08	+37 32 17.0	1953.107	1996.282	18.22	17.44	0.78	17.92	17.44	0.48	1.69	1.20	0.454	-24.9	30.9	0.47	
08 49 02.57	+30 02 35.0	1954.022	1996.282	16.59	16.67	-0.08	16.37	16.65	-0.28	1.02	1.26	0.660	-26.6	31.1	0.00	
08 55 08.94	+34 14 41.2	1955.277	1996.282	19.03	18.32	0.71	18.13	17.59	0.54	1.21	1.25	0.998	-25.9	31.4	0.62	
08 57 21.07	+36 38 44.3	1955.277	1996.282	18.26	17.71	0.55	17.91	17.65	0.26	1.09	0.78	0.450	-24.6	30.7	0.38	
09 00 08.02	+36 46 10.4	1955.277	1996.282	18.11	17.22	0.89	17.70	17.10	0.60	2.67	2.38	0.516	-25.4	31.2	0.57	
09 09 47.85	+31 24 43.2	1955.310	1996.282	18.10	17.89	0.21	16.89	16.68	0.21	1.81	1.50	0.266	-23.2	30.5	0.71	
09 10 54.16	+37 59 14.9	1955.277	1996.282	17.43	17.30	0.13	17.15	17.46	-0.31	250.93	265.93	2.158	-28.8	34.4	2.44	
09 12 06.95	+39 11 45.7	1953.364	1996.282	18.48	18.58	-0.10	17.77	18.14	-0.37	16.98	17.80	1.737	-27.0	33.1	1.81	
09 12 47.80	+28 54 06.0	1955.310	1996.282	18.33	17.78	0.55	17.16	16.79	0.37	1.22	0.88	0.183	-22.5	30.0	0.51	
09 13 28.21	+39 44 43.8	1953.364	1996.282	18.25	18.51	-0.26	17.38	17.55	-0.17	2.06	2.09	1.580	-26.8	32.1	0.86	
09 19 54.30	+29 14 08.5	1955.310	1996.279	17.86	17.96	-0.10	17.61	17.48	0.13	8.10	8.33	0.720	-25.5	32.0	1.33	
09 23 35.46	+31 24 08.2	1955.310	1996.279	18.48	17.88	0.60	17.70	17.34	0.36	4.11	3.35	1.032	-26.4	32.0	0.96	
09 25 54.70	+40 04 14.4	1953.178	1996.279	17.93	17.12	0.81	17.74	17.48	0.26	9.16	9.30	0.471	-25.3	31.7	1.08	
09 29 13.92	+37 57 43.1	1954.022	1996.279	18.30	17.72	0.58	17.59	17.43	0.16	43.19	43.43	1.915	-28.1	33.5	1.84	
09 32 55.46	+28 40 36.6	1952.164	1996.304	16.86	16.66	0.20	16.69	16.66	0.03	1.40	0.94	0.543	-26.1	31.0	0.06	
09 33 11.62	+35 16 27.4	1954.022	1996.304	19.07	17.84	1.23	18.23	17.29	0.94	4.85	4.97	1.121	-26.7	32.1	1.01	
09 33 37.30	+28 45 32.2	1952.164	1996.304	19.39	18.78	0.61	17.86	17.59	0.27	119.85	120.71	3.425	-28.4	34.4	2.61	
09 34 07.29	+35 42 37.6	1954.022	1996.304	17.70	17.71	-0.01	17.11	16.95	0.16	3.87	5.75	1.097	-26.7	32.2	1.03	core-jet 12s
09 35 31.59	+35 41 00.9	1954.022	1996.304	17.56	17.34	0.22	16.95	16.82	0.13	1.54	2.10	0.492	-25.2	31.1	0.52	
09 36 21.52	+39 21 31.8	1953.178	1997.184	19.25	17.93	1.32	17.80	17.32	0.48	27.15	28.51	0.210	-22.7	31.5	1.93	
09 37 04.05	+29 37 04.3	1952.164	1996.304	17.93	17.72	0.21	17.62	17.40	0.22	2.45	2.65	0.452	-24.6	31.1	0.77	FRII 160s
09 41 46.88	+35 30 35.9	1954.022	1996.304	18.63	18.16	0.47	17.66	17.46	0.20	1.12	0.93	0.188	-22.2	30.0	0.62	
09 42 58.10	+40 10 14.2	1953.178	1997.184	18.62	17.51	1.11	17.65	17.12	0.53	1.73	2.02	1.013	-26.8	31.7	0.50	
09 46 10.97	+32 23 25.8	1952.164	1997.186	17.54	17.25	0.29	17.13	17.00	0.13	1.41	1.56	0.403	-24.8	30.8	0.36	
09 47 12.03	+34 51 19.9	1955.279	1996.304	17.73	17.76	-0.03	16.94	16.95	-0.01	1.04	1.20	1.453	-27.4	31.7	0.33	
09 48 55.35	+40 39 44.8	1953.178	1996.304	18.37	17.49	0.88	18.00	17.35	0.65	1439.97	1537.07	1.247	-27.3	34.7	3.35	
09 53 27.98	+32 25 51.7	1955.279	1996.304	17.74	17.05	0.69	17.05	16.73	0.32	128.43	131.85	1.574	-28.3	33.8	2.08	
09 53 31.60	+39 17 30.3	1953.178	1996.304	17.27	17.12	0.15	16.79	16.94	-0.15	4.97	4.45	0.917	-26.9	32.0	0.75	
09 55 37.96	+33 35 04.0	1955.279	1996.304	17.79	17.37	0.42	17.44	17.10	0.34	35.73	36.61	2.499	-29.1	33.7	1.58	
09 55 55.71	+35 16 52.5	1955.279	1996.304	18.46	17.56	0.90	17.59	17.19	0.40	9.28	9.71	1.620	-27.8	32.7	1.15	
09 58 20.95	+32 24 02.6	1955.279	1996.304	16.06	15.81	0.25	15.88	15.93	-0.05	1204.19	1228.71	0.533	-26.9	33.9	2.66	
10 02 02.11	+37 42 24.3	1955.279	1996.307	18.73	18.10	0.63	19.30	17.84	1.46	9.51	8.19	1.799	-27.6	32.8	1.34	
10 02 08.16	+34 53 53.7	1955.279	1996.307	18.74	18.36	0.38	17.05	16.88	0.17	5.58	5.30	0.205	-22.2	30.7	1.39	
10 02 54.50	+32 40 39.6	1955.279	1996.307	18.19	17.11	1.08	17.47	17.05	0.42	9.09	9.00	0.830	-26.7	32.1	1.01	
10 04 10.20	+37 28 48.7	1955.279	1996.515	18.67	17.97	0.70	18.06	17.								

TABLE 2—*Continued*

RA (1)	Dec (2)	POSS1 obs (3)	CCD obs (4)	B (5)	O (6)	B-O (7)	R (8)	E (9)	R-E (10)	S_p (11)	S_i (12)	z (13)	M(B) (14)	L(R) (15)	$\log R^*$ (16)	Morpho (17)
10 10 00.70	+30 03 21.6	1955.373	1996.304	* 17.39	16.59	0.80	16.76	16.20	0.56	1.54	0.99	0.255	-24.5	30.4	0.12	
10 10 27.58	+41 32 38.4	1953.288	1996.307	16.45	16.04	0.41	16.28	16.03	0.25	258.74	340.26	0.613	-27.0	33.5	2.19	FRII 32
10 15 05.77	+36 04 52.9	1954.334	1996.518	18.50	17.94	0.56	17.88	17.55	0.33	29.51	29.85	0.846	-25.9	32.7	1.86	
10 18 58.57	+34 36 32.4	1954.334	1997.268	17.41	16.92	0.49	16.19	16.04	0.15	2.27	2.44	0.109	-22.2	29.8	0.48	
10 20 41.12	+39 58 11.1	1953.288	1996.518	19.45	18.58	0.87	18.36	17.63	0.73	2.71	2.38	0.826	-25.2	31.6	1.08	FRII 16
10 21 17.55	+34 37 22.0	1954.334	1996.526	17.54	17.34	0.20	17.09	17.19	-0.10	317.10	392.03	1.407	-27.7	34.2	2.68	FRII 22
10 21 56.57	+30 01 40.6	1955.364	1996.304	18.29	18.56	-0.27	17.48	17.21	0.27	1.43	1.41	3.115	-28.4	32.4	0.62	
10 22 30.33	+30 41 04.7	1955.364	1996.304	17.58	17.32	0.26	17.07	17.01	0.06	907.01	919.28	1.320	-27.6	34.5	3.05	
10 22 37.38	+39 31 50.6	1953.288	1996.526	17.25	16.93	0.32	16.64	16.32	0.32	41.28	57.53	0.607	-26.1	32.7	1.77	FRII 36
10 23 11.52	+39 48 15.1	1953.288	1996.526	18.17	17.29	0.88	17.52	16.81	0.71	807.88	1078.67	1.252	-27.5	34.6	3.12	
10 23 33.46	+39 53 12.5	1953.288	1997.186	18.36	17.67	0.69	17.80	17.43	0.37	62.13	65.13	1.330	-27.3	33.4	2.04	
10 26 17.50	+30 36 42.7	1955.364	1997.186	18.55	18.12	0.43	17.47	17.25	0.22	1.74	1.82	0.340	-23.6	30.7	0.79	
10 30 45.22	+25 55 22.4	1955.359	1997.268	* 17.47	17.22	0.25	16.92	16.21	0.71	47.56	49.15	0.691	-26.1	32.7	1.81	core-jet
10 30 59.11	+31 02 55.7	1955.364	1997.186	16.29	16.15	0.14	15.88	15.68	0.20	58.74	63.45	0.178	-24.1	31.7	1.57	FRII 30
10 33 03.77	+41 16 05.8	1953.263	1997.186	19.04	18.27	0.77	18.23	17.49	0.74	406.68	432.65	1.120	-26.2	34.1	3.12	
10 33 59.48	+35 55 08.5	1954.334	1997.186	17.12	16.80	0.32	16.41	16.35	0.06	2.06	2.23	0.169	-23.3	30.2	0.38	
10 36 48.48	+37 03 07.1	1954.334	1997.268	18.47	17.77	0.70	18.15	18.24	-0.09	26.23	26.71	1.592	-27.6	33.2	1.67	
10 38 48.12	+37 29 24.0	1954.334	1997.268	17.50	17.44	0.06	17.05	17.51	-0.46	17.47	17.46	0.730	-26.0	32.3	1.44	FRII 68
10 38 59.61	+42 27 42.1	1953.263	1997.268	18.49	18.52	-0.03	17.29	17.32	-0.03	2.76	2.44	0.220	-22.2	30.5	1.15	
10 52 50.06	+33 55 05.1	1953.427	1997.189	17.67	16.95	0.72	16.82	16.77	0.05	12.81	13.41	1.408	-28.1	32.8	1.06	FRII 33
11 02 11.87	+28 40 40.9	1955.304	1997.189	17.46	17.44	0.02	16.64	16.81	-0.17	46.17	48.36	1.741	-28.1	33.5	1.79	
11 03 13.34	+30 14 42.9	1955.304	1997.189	18.18	17.65	0.53	17.64	17.90	-0.26	107.68	108.99	0.387	-24.3	32.6	2.37	FRII 75
11 06 05.69	+30 51 08.5	1955.304	1997.189	17.45	17.10	0.35	16.86	16.80	0.06	1.69	1.92	1.638	-28.3	32.0	0.26	
11 10 40.21	+30 19 09.9	1955.304	1997.189	18.97	17.98	0.99	18.24	17.86	0.38	20.08	22.77	1.522	-27.3	33.1	1.69	FRII 48
11 22 41.49	+30 35 35.1	1950.425	1997.189	17.65	17.01	0.64	16.74	16.74	-0.00	10.06	10.02	1.809	-28.7	32.8	0.93	
11 31 09.29	+26 32 08.1	1950.425	1997.595	16.96	16.44	0.52	16.40	15.46	0.94	2.00	2.72	0.243	-24.5	30.6	0.31	
12 02 43.54	+37 35 52.0	1956.430	1997.578	* 18.48	17.54	0.94	17.77	17.36	0.41	16.29	17.24	1.194	-27.1	32.7	1.43	
12 04 37.56	+28 51 25.1	1955.373	1997.578	17.36	17.07	0.29	16.64	16.51	0.13	6.24	5.57	1.129	-27.5	32.2	0.80	
13 10 59.41	+32 33 34.6	1950.449	1996.279	20.96	16.79	4.17	20.56	16.11	4.45	243.42	245.97	1.650	-28.7	34.2	2.24	
13 11 31.98	+37 34 08.1	1950.449	1996.304	17.31	17.11	0.20	17.11	16.83	0.28	1.20	1.53	1.272	-27.7	31.7	0.19	
13 12 17.75	+35 15 20.6	1950.449	1996.304	15.55	15.66	-0.11	15.05	14.86	0.19	43.92	44.72	0.183	-24.6	31.5	1.22	
13 14 23.14	+29 10 01.7	1955.367	1996.304	* 18.73	18.30	0.43	17.90	17.52	0.38	7.53	7.22	1.094	-26.2	32.3	1.38	
13 26 29.06	+36 23 34.3	1950.452	1996.696	18.10	17.60	0.50	17.63	17.23	0.40	1.75	1.07	0.389	-24.4	30.8	0.56	
13 31 08.31	+30 30 32.9	1950.507	1996.304	17.49	17.38	0.11	17.14	17.11	0.03	14777.96	15023.95	0.848	-26.5	35.4	4.34	
13 33 09.74	+36 20 30.4	1950.452	1996.701	17.95	17.46	0.49	18.53	17.38	1.15	16.63	17.50	0.679	-25.9	32.3	1.46	core-jet
13 34 03.81	+37 01 04.0	1950.452	1996.696	18.38	17.65	0.73	17.45	17.05	0.40	13.17	13.31	1.765	-28.0	32.9	1.31	
13 41 59.89	+37 07 10.5	1950.452	1996.701	17.16	16.67	0.49	17.84	16.61	1.23	24.50	25.42	1.106	-27.8	32.8	1.26	
13 42 54.40	+28 28 06.1	1950.507	1996.515	18.50	18.20	0.30	17.83	17.77	0.06	65.57	68.41	1.040	-26.1	33.2	2.30	FRII 33
13 43 00.18	+28 44 07.3	1950.507	1996.515	17.23	17.00	0.23	16.77	16.43	0.34	217.37	246.65	0.905	-27.0	33.7	2.40	
13 48 04.37	+28 40 25.6	1958.373	1996.515	18.00	17.89	0.11	17.77	17.60	0.17	72.45	78.07	2.464	-28.5	34.0	2.12	
13 48 20.89	+30 20 05.3	1958.373	1996.515	17.36	18.09	-0.73	16.66	17.57	-0.91	22.49	23.53	1.865	-27.7	33.2	1.72	core-jet
13 53 26.08	+36 20 49.6	1950.452	1996.518	16.30	15.90	0.40	15.97	15.63	0.34	1.70	1.57	0.286	-25.4	30.5	-0.12	
13 55 29.94	+29 30 58.9	1958.373	1996.518	18.25	18.47	-0.22	17.43	17.33	0.10	1.74	1.54	0.302	-23.0	30.6	0.91	
14 10 36.79	+29 55 50.7	1958.373	1996.518	18.61	17.69	0.92	18.14	17.76	0.38	4.00	4.09	0.570	-25.2	31.5	0.93	
14 15 28.45	+37 06 21.7	1950.447	1996.518	* 18.20	18.37	-0.17	17.76	17.45	0.31	406.30	409.69	2.360	-27.9	34.7	3.04	
14 23 26.09	+32 52 20.6	1950.466	1997.496	17.25	16.67	0.58	16.16	16.23	-0.07	8.71	8.16	1.903	-29.1	32.8	0.72	
14 25 50.71	+24 04 03.5	1950.299	1997.496	* 17.93	17.78	0.15	17.13	17.14	-0.01	121.14	320.88	0.654	-25.4	33.5	2.85	FRII 22
14 31 20.55	+39 52 41.8	1950.532	1996.523	* 16.47	16.68	-0.21	15.87	15.69	0.18	207.87	210.04	1.217	-28.0	33.8	2.17	
14 37 19.19	+38 04 38.1	1950.466	1996.690	18.24	17.57	0.67	17.75	17.41	0.34	34.25	35.08	1.043	-26.8	32.9	1.76	
14 37 56.48	+35 19 36.8	1950.466	1996.526	18.16	17.85	0.31	17.95	17.42	0.53	16.53	53.48	0.537	-24.9	32.5	2.12	FRII 20
14 55 43.46	+30 03 22.6	1955.364	1996.282	* 17.39	16.69	0.70	16.94	16.21	0.73	1.80	1.41	0.626	-26.4	31.2	0.17	
15 14 43.03	+36 50 50.4	1956.499	1996.282	16.49	15.78	0.71	16.30	15.87	0.43	48.97	70.99	0.369	-26.1	32.3	1.44	FRII 60
15 17 28.49	+28 56 15.8	1954.564	1996.282	18.65	17.86	0.79	17.53	17.40	0.13	1.39	0.84	0.208	-22.7	30.1	0.59	
15 19 36.16	+28 38 27.0	1954.564	1996.282	17.22	17.37	-0.15	16.61	16.75	-0.14	2.08	1.99	0.269	-23.8	30.5	0.56	
15 23 14.50	+37 59 28.4	1950.447	1996.690	18.29	18.44	-0.15	17.43	17.64	-0.21	1.67	1.83	1.344	-26.5	31.9	0.80	
15 25 23.58	+42 01 17.1	1955.329	1996.523	18.43	18.47	-0.04	17.74	17.64	0.10	104.19	122.19	1.198	-26.2	33.6	2.65	core-jet
15 29 18.04	+32 48 42.3	1950.447	1996.690	17.70	17.52	0.18	17.05	16.99	0.06	28.91	29.62	1.652	-27.9	33.2	1.61	
15 30 45.79	+38 39 52.7	1955.329	1996.282	18.54	17.91	0.63	17.82	17.36	0.46	2.28	2.28	2.035	-28.0	32.3	0.62	
15 37 30.98	+33 58 36.1	1950.447	1996.696	18.34	17.74	0.60	17.22	17.43	-0.21	5.27	5.58	1.025	-26.6	32.1	1.03	
15 40 42.98	+41 38 16.0	1955.329	1996.696	17.70	17.93	-0.23	17.28	17.15	0.13	17.67	18.28	2.506	-28.5	33.4	1.51	
15 42 27.03	+29 42 02.4	1950.460	1996.282	18.55	18.10	0.45	17.88	17.64	0.24	1.54	1.35	0.457	-24.3	30.9	0.69	
15 42 41.12	+29 34 28.9	1950.460	1996.282	18.68	18.19	0.49	17.99	17.90	0.09	1.58	1.81	1.098	-26.3	31.7	0.72	
15 43 48.62	+40 13 24.8	1955.329	1997.578	17.91	17.72	0.19	17.14	16.79	0.35	3.24	2.75	0.318	-23.8	30.9	0.88	
15 44 05.61	+32 40 49.1	1950.447	1997.578	17.70	17.92	-0.22	17.04	17.52	-0.48	210.79	213.88	1.047	-26.4	33.7	2.69	
15 45 12.93	+30 05 08.0	1950.460	1996.523	18.50	19.24	-0.74	17.71	17.83	-0.12	6.73	6.26	0.322	-22.3	31.2	1.81	
15 48 17.94	+35 11 27.5	1950.359	1996.523	18.26	18.04	0.22	17.92	17.70	0.22	140.94	141.51	0.479	-24.5	32.9	2.63	

TABLE 2—*Continued*

RA (1)	Dec (2)	POSS1 obs (3)	CCD obs (4)	B (5)	O (6)	B-O (7)	R (8)	E (9)	R-E (10)	S_p (11)	S_i (12)	z (13)	M(B) (14)	L(R) (15)	log R^* (16)	Morphology (17)
16 11 23.26	+29 59 47.2	1950.512	1996.526	18.50	18.56	-0.06	17.85	17.75	0.10	1.69	1.90	1.711	-27.0	32.1	0.83	core-jet
16 13 41.09	+34 12 48.3	1954.564	1996.526	18.11	17.74	0.37	17.23	17.53	-0.30	3532.04	3605.54	1.404	-27.3	35.2	3.81	
16 14 36.84	+28 39 06.2	1950.512	1996.523	19.39	19.05	0.34	17.80	17.51	0.29	2.22	1.31	0.316	-22.5	30.7	1.25	
16 19 02.43	+30 30 51.4	1950.512	1996.526	17.24	17.29	-0.05	16.56	16.46	0.10	66.82	67.58	1.284	-27.5	33.4	1.91	
16 23 07.39	+30 04 06.2	1954.567	1996.526	18.08	17.29	0.79	17.32	16.95	0.37	1.65	1.04	1.165	-27.3	31.7	0.31	FR II 22s
16 23 19.92	+41 17 02.8	1953.460	1997.496	17.46	17.32	0.14	16.64	16.67	-0.03	3.23	2.98	1.618	-28.1	32.3	0.57	
16 23 30.56	+35 59 32.8	1954.564	1996.526	18.55	17.91	0.64	17.90	17.59	0.31	259.58	266.83	0.867	-26.0	33.6	2.80	
16 24 22.02	+39 24 41.5	1953.460	1996.526	18.94	18.31	0.63	18.26	17.76	0.50	132.32	144.52	1.117	-26.2	33.6	2.66	
16 25 48.78	+26 46 58.5	1954.567	1997.595	17.40	17.09	0.31	17.01	17.05	-0.04	10.12	9.69	2.521	-29.4	33.1	0.91	FR II 20s
16 26 59.26	+30 15 34.9	1954.567	1996.526	18.36	18.17	0.19	17.55	17.19	0.36	5.34	5.42	1.582	-27.2	32.5	1.14	
16 29 01.32	+40 08 00.0	1953.460	1996.526	17.67	18.11	-0.44	17.25	17.86	-0.61	11.97	11.94	0.271	-23.1	31.3	1.61	
16 30 20.76	+37 56 56.2	1954.564	1996.690	16.59	17.31	-0.72	16.43	17.45	-1.02	20.00	21.73	0.395	-24.7	31.9	1.53	
16 33 02.11	+39 24 27.5	1953.460	1996.690	17.17	16.86	0.31	16.56	15.97	0.59	41.29	54.38	1.021	-27.4	33.1	1.67	FR II 20s
16 33 48.99	+31 34 11.8	1954.567	1996.690	17.38	17.72	-0.34	16.87	17.27	-0.40	1.79	2.07	1.516	-27.5	32.0	0.55	
16 34 02.97	+39 00 00.7	1953.460	1996.690	18.91	18.38	0.53	18.22	18.03	0.19	915.40	931.91	1.085	-26.1	34.4	3.51	
16 34 12.78	+32 03 35.2	1954.567	1996.515	17.61	17.26	0.35	17.23	16.77	0.46	175.25	176.52	2.341	-29.0	34.3	2.23	
16 35 15.46	+38 08 04.1	1954.564	1996.690	17.08	17.83	-0.75	16.33	17.61	-1.28	2653.87	2694.06	1.811	-27.8	35.3	3.68	core-jet 1
16 37 09.33	+41 40 30.4	1953.460	1996.690	16.95	17.38	-0.43	16.64	17.05	-0.41	7.37	7.11	0.765	-26.2	32.0	1.04	
16 39 31.75	+39 08 45.7	1953.460	1996.690	18.36	17.91	0.45	17.46	17.28	0.18	1.27	0.72	0.143	-21.8	29.8	0.58	
16 40 29.62	+39 46 46.2	1953.460	1996.690	19.37	18.64	0.73	18.59	17.96	0.63	1088.22	1108.55	1.670	-26.8	34.8	3.63	
16 41 54.24	+40 00 33.0	1953.460	1997.595	18.10	17.99	0.11	17.63	17.68	-0.05	6.89	5.06	1.003	-26.3	32.2	1.23	core-jet 1
16 42 18.96	+31 54 33.9	1954.567	1996.611	18.55	18.21	0.34	17.93	17.78	0.15	23.08	24.01	1.263	-26.6	32.9	1.83	
16 42 58.78	+39 48 37.1	1953.460	1996.690	17.62	16.19	1.43	17.12	15.69	1.43	6050.06	6598.61	0.595	-26.8	34.7	3.54	
16 43 47.87	+30 11 08.6	1954.567	1996.699	17.67	17.45	0.22	17.00	16.77	0.23	1.42	1.38	1.380	-27.6	31.8	0.29	
16 50 05.45	+41 40 32.3	1953.460	1996.690	17.85	17.18	0.67	17.46	17.33	0.13	170.28	185.19	0.584	-25.8	33.2	2.38	complex
16 52 52.62	+36 00 57.3	1954.482	1996.696	18.53	18.80	-0.27	17.68	17.71	-0.03	1.36	2.22	0.281	-22.5	30.6	1.16	
16 52 55.92	+31 23 43.5	1950.466	1996.699	17.79	17.94	-0.15	17.51	17.87	-0.36	1.16	1.47	0.590	-25.0	31.1	0.58	
16 55 00.24	+30 30 40.0	1950.466	1996.699	18.21	17.63	0.58	17.66	17.34	0.32	3.20	2.86	0.405	-24.5	31.1	0.83	
16 55 57.40	+32 18 05.3	1950.466	1996.699	18.34	18.19	0.15	17.51	17.42	0.09	1.10	1.19	1.327	-26.7	31.7	0.51	core-jet 1
16 57 22.12	+39 55 51.7	1954.597	1996.699	17.89	17.83	0.06	17.50	17.45	0.05	1.19	0.77	0.579	-25.1	31.0	0.45	
16 59 24.14	+26 29 37.0	1955.329	1997.595	* 18.55	18.21	0.34	18.07	17.90	0.17	391.07	538.46	0.794	-25.5	33.9	3.23	
16 59 31.91	+37 35 28.4	1954.482	1996.699	17.45	17.34	0.11	17.14	17.41	-0.27	18.31	18.57	0.775	-26.3	32.4	1.42	
17 02 31.01	+32 47 20.6	1954.482	1996.526	16.21	16.09	0.12	15.71	16.03	-0.32	1.82	1.52	0.163	-23.9	30.0	0.01	FR II 56s
17 06 48.07	+32 14 22.7	1950.466	1996.690	16.87	17.06	-0.19	16.27	16.46	-0.19	36.32	38.71	1.070	-27.3	33.0	1.60	
17 08 23.08	+41 23 09.4	1954.597	1996.699	17.36	17.26	0.10	17.08	16.85	0.23	1.23	0.94	0.837	-26.5	31.3	0.21	
17 10 13.50	+33 44 03.3	1954.592	1997.496	16.45	15.93	0.52	15.64	15.25	0.39	4.05	4.60	0.208	-24.7	30.7	0.34	
17 13 04.48	+35 23 33.8	1954.592	1996.526	16.95	16.80	0.15	15.99	15.85	0.14	11.13	11.24	0.083	-21.7	30.2	1.10	FR II 130s
17 16 01.95	+31 12 13.7	1950.540	1996.526	15.93	15.39	0.54	15.30	14.61	0.69	2.68	2.42	0.110	-23.8	29.9	-0.09	
17 16 54.19	+30 27 01.4	1950.540	1997.496	17.45	17.07	0.38	16.87	16.74	0.13	4.25	3.96	0.751	-26.5	31.7	0.68	
17 19 34.17	+25 10 58.7	1951.589	1997.595	16.36	16.57	-0.21	15.74	15.76	-0.02	12.67	13.83	0.579	-26.4	32.0	1.01	
17 20 07.69	+36 54 39.2	1954.592	1997.595	17.75	17.82	-0.07	16.91	16.87	0.04	3.42	3.34	0.332	-23.8	30.9	0.94	FR II 200s
17 21 09.50	+35 42 16.2	1954.592	1996.688	19.12	17.14	1.98	17.93	16.58	1.35	386.51	392.99	0.283	-24.1	32.9	2.74	
17 23 20.79	+34 17 57.6	1954.592	1996.688	15.77	15.16	0.61	15.48	14.96	0.52	438.57	441.20	0.205	-25.4	32.6	2.01	
17 23 54.30	+37 48 41.1	1954.592	1996.690	17.72	18.43	-0.71	17.13	17.64	-0.51	1.70	1.72	0.828	-25.4	31.4	0.82	
17 26 32.71	+39 57 02.1	1953.529	1996.688	18.40	18.49	-0.09	18.06	18.00	0.06	475.49	496.89	0.656	-24.7	33.7	3.33	core-jet 1
17 26 35.10	+32 13 23.0	1950.540	1996.699	17.99	17.78	0.21	17.36	17.24	0.12	120.94	123.67	1.094	-26.7	33.5	2.39	
17 28 59.09	+38 38 26.0	1954.592	1996.688	17.06	16.86	0.20	16.53	16.76	-0.23	240.27	245.41	1.391	-28.2	34.0	2.29	
17 34 03.52	+40 37 54.0	1953.529	1997.595	17.27	16.50	0.77	16.38	15.91	0.47	1.07	2.53	0.356	-25.3	30.9	0.28	
21 35 13.10	-00 52 43.8	1954.589	1996.688	18.49	17.96	0.53	17.88	17.66	0.22	1.84	1.32	1.660	-27.5	32.0	0.58	FR II 55s
21 36 38.60	+00 41 54.5	1954.589	1996.688	17.20	17.25	-0.05	16.72	16.65	0.07	3546.71	3712.01	1.930	-28.6	35.5	3.58	
21 37 48.50	+00 12 20.5	1954.589	1996.688	18.40	18.14	0.26	17.92	17.72	0.20	36.02	39.56	1.666	-27.3	33.4	1.98	
21 59 24.09	+01 13 05.3	1954.652	1996.701	17.05	16.57	0.48	16.24	15.69	0.55	1.45	2.10	1.000	-27.7	31.7	0.14	
22 01 03.12	-00 52 59.6	1954.652	1996.701	17.34	16.73	0.61	16.24	16.10	0.14	1.47	1.58	0.213	-23.9	30.2	0.19	core-jet 8
22 03 14.81	-01 31 23.4	1954.652	1996.701	16.78	16.51	0.27	16.46	16.24	0.22	14.21	14.25	0.650	-26.7	32.1	0.99	
22 03 55.60	+00 55 16.7	1954.652	1996.718	18.65	17.70	0.95	18.08	17.31	0.77	2.75	2.49	0.720	-25.8	31.5	0.75	
22 06 25.99	-01 52 01.1	1954.652	1996.718	18.35	18.14	0.21	17.18	17.17	0.01	2.60	2.97	1.110	-26.3	31.9	0.91	
22 18 06.66	+00 52 23.9	1954.652	1996.929	16.56	17.28	-0.72	16.12	16.86	-0.74	53.42	54.77	1.270	-27.5	33.3	1.82	core-jet 8
23 44 03.12	+00 38 03.9	1951.989	1996.696	17.27	16.68	0.59	16.82	16.58	0.24	1.57	1.65	1.230	-28.1	31.7	0.06	
23 55 20.58	+00 07 48.0	1951.989	1996.934	18.56	18.22	0.34	17.78	17.83	-0.05	17.72	18.92	1.070	-26.2	32.7	1.75	core-jet 8

NOTE.—Descriptions of table columns:

Cols 1–2: FIRST radio positions (J2000).

Col 3: Date of POSS-I observation.

Col 4: Date of CCD observation.

Cols 5–10: Extinction-corrected CCD magnitudes (B, R), POSS-I magnitudes (O, E) and colors. An asterisk preceding B indicates sources with too few CCD calibration stars to recalibrate the POSS-I magnitudes (see text.)

Cols 11–12: 20 cm peak (col. 11) and integrated (col. 12) flux densities in mJy from the FIRST catalog.

Col 13: Redshift.

Col 14: Absolute B magnitude.

Col 15: Log of radio luminosity ($\text{erg cm}^{-2} \text{s}^{-1} \text{Hz}^{-1}$) at a rest-frame frequency of 5 GHz, assuming spectral index $\alpha = -0.5$ ($F_\nu \propto \nu^\alpha$).Col 16: K -corrected 5 GHz radio to 2500 Å optical luminosity ratio using the definition of Stocke et al. (1992).

Col 17: Radio morphology. Categories are FR II (double, with approximate separation), core-jet (with approximate jet length), and complex. Objects with no notation are symmetrical, isolated sources.